Candidate drugs binding the Anaphase Promoting Complex: A novel target for anti-cancer therapy

Douglas J. Saforo, Brian C. Sils, and J. Christopher States
Pharmacology and Toxicology, University of Louisville School of Medicine

Abstract

Spindle poisons (e.g. paclitaxel) induce mitotic arrest and apoptosis in cancer cells. The anaphase promoting complex/cyclosome (APC/C) is an E3 ubiquitin ligase and the master regulator of cell cycle progression. Activation of the spindle assembly checkpoint (SAC) by spindle poisons inhibits the APC/C and induces mitotic arrest. Spindle poisons depend on functional SAC to induce mitotic arrest. Direct inhibition of the APC/C obviates the need for a functional SAC. Homology structure models for interacting APC/C subunits ANAPC11 and ANAPC2 were used for *in silico* screening of ANAPC2 to identify compounds predicted to interfere with ANAPC11 binding. Previous studies showed 3 compounds induced mitotic arrest and apoptosis in carcinoma cells but not in telomerase immortalized human fibroblasts. Thermal denaturation assay of recombinant protein can confirm on-target binding. Expressing recombinant 6XHis tagged ANAPC2 failed. The ANAPC2 cassette was then ligated into a new expression system utilizing a chitin-binding affinity tag and intein mediated purification. C-terminal (pTXB1-X10) and N-terminal (pTYB21-Y8) fusion constructs were prepared and tested in three expression hosts and evaluated for optimal yield. Large scale preparation of recombinant ANAPC2 using *E.coli* host BL21 expressing the N-terminal fusion protein is in progress. Compound binding to purified recombinant ANAPC2 will be determined. Compound binding of ANAPC2 will indicate that compounds targeting the APC/C can induce mitotic arrest and kill cancer cells while sparing normal cells and may be an effective approach to developing new anti-cancer drugs. Supported by National Cancer Institute grant R25-CA-134283.

Introduction

Cancer, a disease of unchecked cellular proliferation, is the second leading cause of death in the U.S., killing over 1,500 people a day. World wide cancer deaths reached 7.6 million in 2008. Although it is lower on the list of causes of death in developing countries, cancer rates have slowly risen as life expectancies increase.

In the US, survival rates have improved largely due to better detection and early treatment of the disease, not because of more effective chemotherapeutics. However, a growing number of patients are encountering cancers that simply can't be eradicated with the traditional chemotherapeutics.

Paclitaxel, a widely used drug for several types of cancer, disrupts mitotic spindle function through tubulin stabilization/destruction. This route of treatment relies on a functional spindle assembly checkpoint (SAC) that can signal the cell to pause in mitosis due to incorrect alignment/tension of sister chromatids at the metaphase plate. One function of the SAC is to inhibit the anaphase promoting complex/cyclosome (APC/C) which is the master regulator of mitotic progression.

Many cancers resistant to paclitaxel lack a functional SAC. Other cancers can develop mutations spontaneously in the genes encoding the complex pathway that makes up the SAC. By developing a new class of chemotherapeutics that directly target the APC/C, bypassing the SAC, defects in the SAC will not limit the efficacy of treatment.

Anaphase Promoting Complex

- An E3-Ubiquitin Ligase, responsible for the transfer of ubiquitin molecules to a protein target via an isopeptide bond to a lysine side chain followed by elongation of the ubiquitin chain.
- Composed of eleven subunits and two potential activating proteins.
- Catalytic subunit ANAPC11 (a zinc RING finger protein), Scaffolding subunit ANAPC2 (a cullin-like protein), and Activator proteins CDC20 or CDH1 are responsible for selective enzymatic function.
- Master regulator of mitosis and targets include securin, Cyclin B, Cyclin A, geminin and many others.
- Target protein ubiquitination results in degradation by the 26S proteasome.
- Securin degradation releases separase from securin inhibition and allows it to cleave cohesin. Cohesin acts like a "glue" to hold sister chromatids together.

Hypothesis

If candidate compounds block the binding of subunits of the APC/C and inhibit it, then cancer cells will undergo mitotic arrest and either undergo apoptosis during mitosis or proceed to arrest and undergo apoptosis in early G1.

Methods

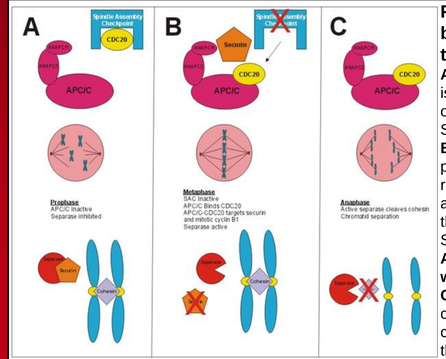

Figure 1. A simplified model of the interaction between the spindle assembly checkpoint and the APC/C during mitosis.
A. In late prophase, the CDC20 co-activator of the APC/C is sequestered by the spindle assembly checkpoint. Pairs of sister chromatids are held together by cohesin. Separase enzyme is inhibited by securin.
B. In metaphase, pairs of sister chromatids have been placed along the metaphase plate by spindle fibers. The requirements of the spindle assembly checkpoint are met, and the CDC20 co-activator is released. CDC-20 binds to the APC/C, enabling it to target securin for degradation. Separase enzyme is activated. **Compound binding of ANAPC2 would inhibit the APC/C, thus separase would remain inactive.**
C. In anaphase, the active separase enzyme cleaves the cohesin protein. This allows separation of the sister chromatids, which begin to move toward polar regions of the dividing cell.

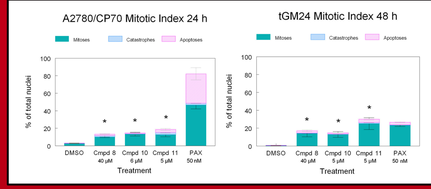

Figure 2. Mitotic index determination. Ovarian cancer cells (A2780/CP70) were treated at the IC50 for compounds 8, 10, and 11 for 24 h. Fibroblasts (tGM24) were treated for 48 h. Paclitaxel was used as a positive control. Slides were prepared for mitotic index and mitotic catastrophe determination. All compounds induced increases in mitotic index in ovarian cancer and diploid fibroblasts. (* = p<0.05)

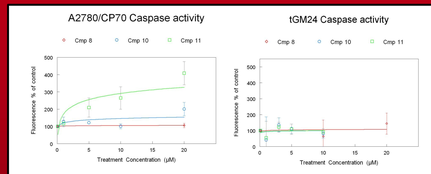

Figure 3. Assessment of caspase 3 activity. Ovarian cancer cells (A2780/CP70 and SKOV3) were plated in a 96-well plate and treated at the indicated concentrations for 24 hours. Fibroblasts (tGM24) were treated for 48 hours. Compounds 10 and 11 induced caspase 3 activity in cancer cells, but not fibroblasts. Compound 8 did not show increase in caspase 3 activity even at high concentrations (Data not shown).

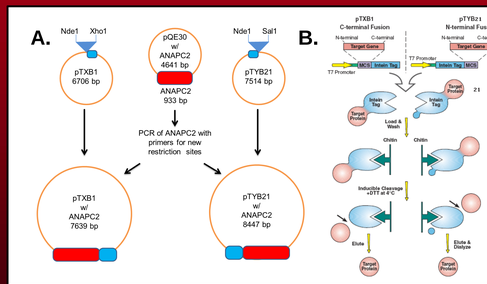

Figure 4. Cloning Strategy. A. The ANAPC2 cassette is transferred from the pQE30 plasmid that utilizes a 6X His tag to the pTXB1 and pTYB21 plasmids that utilize an intein tag. pTXB1 uses restriction site for Nde1 and Xho1. pTYB21 uses restriction sites for Nde1 and Sal1.
B. The fusion protein contains a self-cleaving intein peptide and a chitin binding domain. The fusion protein will bind to a chitin column and intein cleavage is induced with DTT to elute pure protein.
Image obtained from NEB IMPACT™ manual.

Results

Figure 5. DNA amplification and plasmid construction.
A.DNA amplification of ANAPC2 cassette with primers containing restriction sites for new expression system. Sample 3 – Nde1 + Xho1; Sample 4 – Nde1 + Sal1.
B.Gel extraction and PCR product purification from 0.6% agarose gel
C. Verification of the successful sequential restriction digest of plasmid pTXB10 (X10 and X11), and pTYB21 (Y8 and Y9). Overnight ligation of fragments yielded two complete plasmid constructs . Sequencing confirmed proper ligation of the ANAPC2 cassette.
Above: C-terminal fusion of ANAPC2 (~7700 bp)
Below: N-terminal fusion of ANAPC2 (~8500 bp)

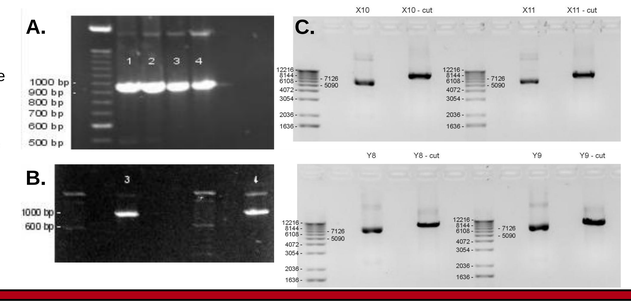

Figure 6. Expression optimization.
Three *E.coli* expressions hosts (ER2566, BL21, T7X (data not shown)) were transformed with plasmids containing C-terminal (X10 and X11) and N-terminal (Y8 and Y9) fusions of the ANAPC2 cassette. 50 mL cultures incubated at 37C and expression was induced by addition of 0.4 mM IPTG. Samples collected every hour to monitor expression. Immunodetection of CBD depicted right. Fusion protein is ~96 kDa. ANAPC2 is ~40 kDa.
A. ER2566 X10 and X11
B. ER2566 Y8 and Y9
C. BL21 X10 and X11
D. BL21 Y8 and Y9

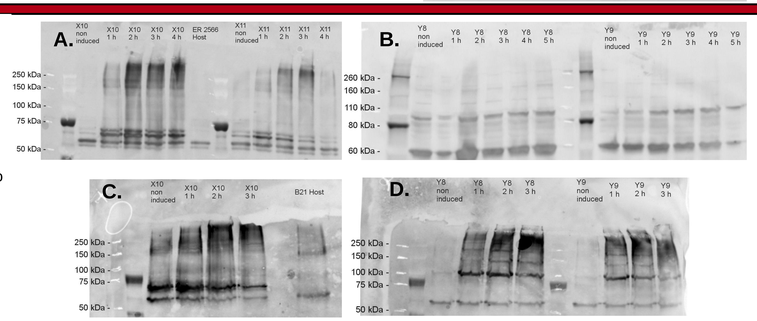

Figure 7. Protein purification. Immunodetection of CBD (left) and ANAPC2 (right). Clarified extract from 4 L culture of pTYB21-Y8 transformed BL21 loaded onto a chitin column. Washed chitin column overnight and induced intein cleavage with 40 mM DTT for 40 h at 4°C. Purified protein collected in fractions and transferred to storage buffer.

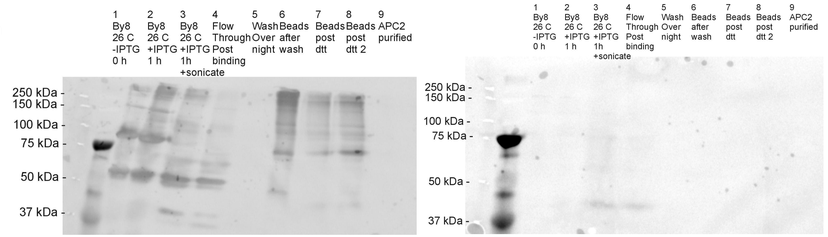

Future Directions

Figure 8. Thermofluor assay
Purified ANAPC2 will be tested by thermofluor assay in order to confirm on-target binding of candidate compounds. Fluorescent dye is added to the purified protein in a 96 well plate and heated.
As the protein the unfolds, the dye binds to hydrophobic regions of the protein and becomes intensely fluorescent. Data are recorded as fluorescence intensity versus temperature.
Definitive shifts in the melting curve will confirm compound binding.

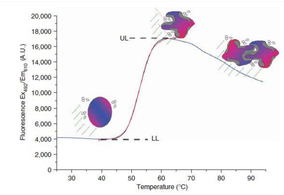

Image obtained from Frank H Niesen, Helena Berglund & Masoud Vedadi Nature Protocols 2 2007.

Conclusions

- Compounds targeting the APC/C induced mitotic arrest in cancer cells and diploid fibroblasts. Activation of caspase 3 in cancer cell lines but not diploid fibroblasts suggests candidate compounds may be developable into cancer-selective drugs.
- The ANAPC2 cassette is successfully ligated into an expression system that expressed an appreciable amount of protein. After purification refinements, a binding study will be viable.
- On-target binding can be determined through high-throughput thermofluor assay. This assay provides a means of testing more candidate compounds in our catalog. If inhibition of APC/C function is verified, the APC/C may be a promising target for future chemotherapeutics.

Acknowledgements

This research was supported in part by the University of Louisville Cancer Education Program NIH/NCI grant R25-CA134283 and a Basic Grant from the UofL School of Medicine.

Endocytic Trafficking of Mutant Epidermal Growth Factor Receptors in Lung Cancer

UNIVERSITY OF LOUISVILLE

Tejas N. Sangoi[1] and Brian P. Ceresa[2]

[1]R25 Cancer Education Program, University of Louisville

[2]Department of Pharmacology and Toxicology, University of Louisville

Abstract

Purpose: To better understand the endocytic pathway and mechanism of how activating T790M mutants of epidermal growth factor receptor (EGFR) regulates signaling in two lung carcinoma cell lines: PC-9 and H1650.

Methods: PC-9 and H1650 cells express mutant EGFRs; HeLa cells express wild type EGFRs. Immunoblotting was used to test for time-dependent EGFR phosphorylation and degradation. Receptor trafficking and endosomal accumulation was observed by immunofluorescence staining of the EGFR. Kinetics of 125I-EGF endocytosis and ligand-mediated degradation was measured by radioligand binding assay.

Results: Immunoblotting shows that EGF treatment causes an increase in the basal activity of EGFR phosphorylation, and peaks at 30 minutes. Immunofluorescent staining of the EGFR indicates that a substantial amount of the unliganded, mutant EGFR accumulates in the early endosome and EGF treatment further increases endosomal accumulation in the mutant EGFR. Furthermore, there is a slower rate of receptor degradation of the mutant EGFRs compared to wild type receptor, as seen in the radioligand binding assay.

Conclusions: Activating mutants of EGFRs found in lung cancer cells not only have higher basal phosphorylation, but also defective endocytic trafficking. Based on radioligand binding and immunofluorescence experiments, it can be concluded that the receptor trafficking defect causes increased receptor accumulation in the endosome. Less degradation in the cancer cell lines indicates there is a disruption in the endocytic trafficking of mutant EGFRs.

Introduction

- Lung cancer is a major health concern in the Commonwealth of Kentucky, and there are more deaths in the U.S. from lung cancer than any other cancer. (www.cdc.gov)
- Specifically, over 85% of lung cancers are non-small cell lung cancer (NSCLC), and these cells are used as a model in this project. (www.cancer.org)
- Many NSCLC cells are characterized by activating EGFR mutations.
- EGFR is a receptor tyrosine kinase on the cell surface that is normally activated by ligand binding, and inactivated by either endocytic recycling or degradation.
- Common Mutations found in studies:

Mutation	# of Individuals	Location of Patients	Results	Reference
Exons 18-21	860 total (748 M, 112 W)	Pisa and Chieti, Italy	More frequent in women over men, and in nonsmokers over smokers	①
Exons 18-21	277 total (159 M, 118 W)	Aichi, Japan	More frequent in women over men, and in nonsmokers over smokers	②
L858R, T790M, Exon 19	135 non-smoking women	Shanghai, China	Low ERC11 levels and TS mRNA can affect chemotherapy treatment	③
T790M	31 total	Boston, Massachusetts	Single mutations at multiple cancer sites; multifocal tumors at diff. sites	④
L858R	119 total (58 Japan, 61 U.S.)	Nagoya City, Japan & Boston, Massachusetts	More frequent in women over men, and in Japan over U.S.	⑤

1 A. Marchetti et al., EGFR Mutations in Non-Small-Cell Lung Cancer. *Journal of Clinical Oncology*, 23: 857-865, 2005.
2 T. Kosaka et al., Mutations of the Epidermal Growth Factor Receptor Gene in Lung Cancer. *Journal of Cancer Research*, 64: 8919, 2004.
3 S. Ren et al., Association of EGFR mutation or ALK rearrangement with expression of DNA repair...*Cancer*. 118: 5588-5594, 2012.
4 S. Maheswaran et al., Detection of Mutations in EGFR in Circulating Lung-Cancer Cells. *New England Journal of Medicine*, 359: 366-77, 2008.
5 G. Paez et al., EGFR Mutations in Lung Cancer: Correlation with Clinical Response to Gefitinib Therapy. *Science*, 304: 1497-1500, 2004.

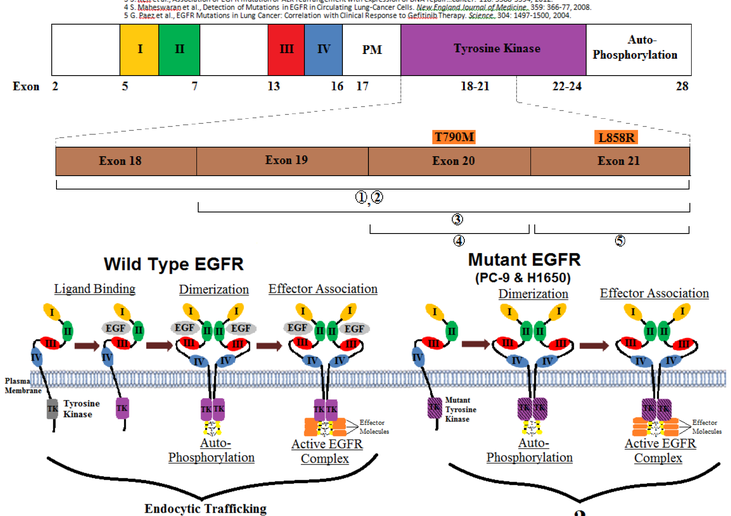

In its unstimulated state, the wild type EGFR is a monomer on the cell surface. Upon ligand binding, the receptor undergoes a conformational change which fosters receptor dimerization and activation of the intracellular kinase domain. Receptor pairs trans-phosphorylate, yielding C-terminal phosphotyrosine; these phosphotyrosine serve as docking sites for downstream signaling proteins. In contrast, the T790M mutant EGFR has constitutive kinase activity, and thus proceeds with the dimerization, auto-phosphorylation, and effector association steps without a ligand present.

Hypothesis

Constitutively active epidermal growth factors have altered endocytic trafficking.

Figure 1

EGFR Phosphorylation and Degradation in PC-9, H1650, and HeLa cells

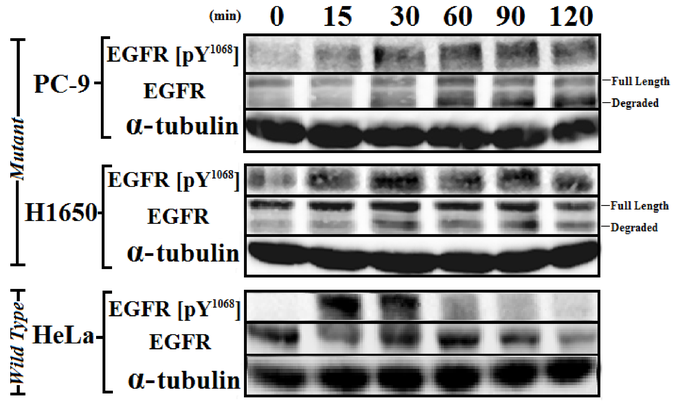

Figure 1. PC-9, H1650, and HeLa cells were serum starved and then treated for 0-120 minutes with 10 ng/mL of epidermal growth factor (EGF). Cell lysates were harvested and equivalent amounts of protein were resolved in a 7.5% SDS-PAGE. Gels were transferred to nitrocellulose and probed for pY1068, EGFR, and α-tubulin. pY1068 is a monoclonal antibody that targets tyrosine 1068, an important auto-phosphorylation site in the cytoplasmic domain of EGFR. The EGFR antibody detects the amount of total EGFR present. α-tubulin is another monoclonal antibody that serves as a loading control. The results shown are representative blots from an experiment performed multiple times.

Figure 2

Immunofluorescence Images of PC-9, H1650, and HeLa cells

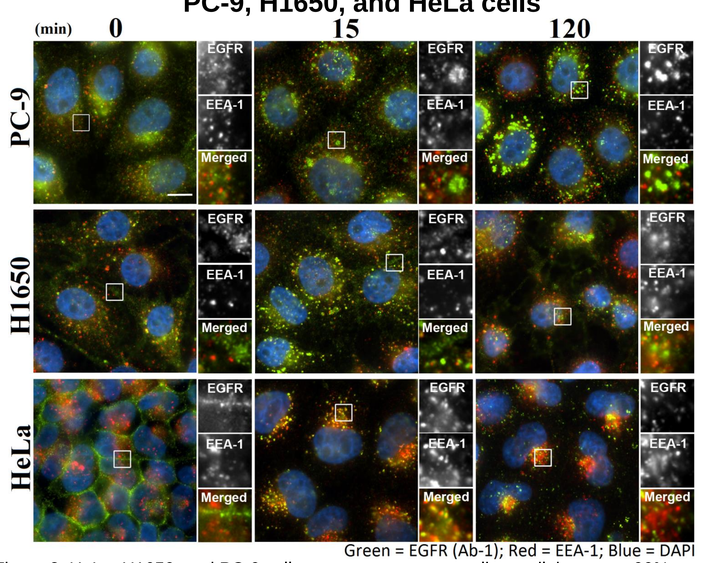

Green = EGFR (Ab-1); Red = EEA-1; Blue = DAPI

Figure 2. HeLa, H1650, and PC-9 cells were grown on coverslips until they were 90% confluent. Cells were treated with 10 ng/mL EGF at 0,15, or 120 minutes. Cells were fixed, permeabilized, probed for EGFR (Ab-1) and EEA-1, and stained prolong with Dapi, an invitrogen product. EGFR (Ab-1) is a monoclonal mouse antibody against EGFR, and EEA-1 is a monoclonal rabbit antibody against early endosome. Scale bar = 10 μm.

Figure 3

^{125}I-EGF Binding Assay

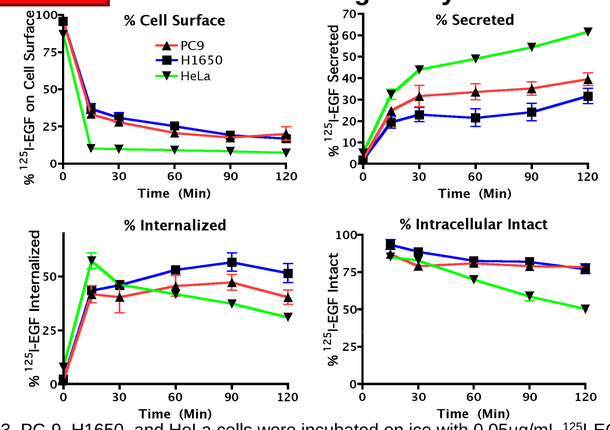

Figure 3. PC-9, H1650, and HeLa cells were incubated on ice with 0.05μg/mL ^{125}I-EGF until steady-state cell surface binding was achieved. Free radioligand was removed and cells were incubated in 37°C media. At each time point, samples were collected to determine the total secreted, cell surface, internalized, and intracellular ^{125}I-EGF. Intracellular ^{125}I-EGF was TCA preceipitated to determine the amount of degraded and intact ^{125}I-EGF.The data shown are average ± S.E.M. PC-9, n=4; H1650, n=3; HeLa, n=2.

Figure 4

Model of T790M EGFR Endocytic Trafficking

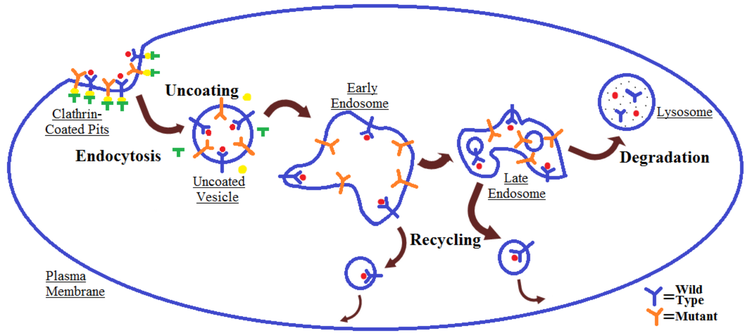

Figure 4. Both wild type and T790M mutant EGFRs enter the cell via clathrin-coated pits. The EGFR is contained in the resulting clathrin-coated vesicles, which shed its clathrin and fuse with an early endosome. Wild type EGFR then gets sorted to either be recycled to the plasma membrane or degraded via the lysosome. Mutant EGFRs appear to accumulate in the endosome.

Conclusions

- Activating mutants of EGFRs in lung cancer cells result in a receptor that is constitutively active, as indicated by the partial phosphorylation.
- There is substantial intracellular accumulation of unliganded EGFRs in lung cancers.
- Addition of ligand further increases receptor accumulation in the endosome.
- Less degradation in the cancer cell lines indicates there is a disruption in the endocytic trafficking of mutant EGFRs.

Future Experiments: determine where T790M localization is occurring, and what effector molecules are allowing sustained activities of EGFR.

Acknowledgements

R25 Cancer Education Program, Joanne Peterson, Jamie Rush, Eileen Parks, Nicole Jackson; **Funding**: NIH/NCI R25-CA134283.

Automated G-Quadruplex Generation: From Sequence To Structure

Nicholas C. Siow[1], Yidi Huang[1], Huy T. Le[2], Jon M. Maguire[1], John O. Trent[1,2,3]
[1] James Graham Brown Cancer Center, [2] Department of Biochemistry and Molecular Biology, [3] Department of Medicine

Abstract

In the search for targeted anti-cancer drugs, the choice of molecular targets is of fundamental importance. Tetrahelical structures known as quadruplexes are formed by sequences of guanine-rich DNA and are promising possible targets due to their highly diverse topologies offering a variety of target sites. While computational models of these structures could be valuable resources, the degree of polymorphism within quadruplex-forming sequences makes manual production of these models a difficult task. Therefore, an automated means of quadruplex generation is a far more attractive solution for representing the full range of variation within quadruplexes. Such a solution would independently alter the quadruplex size, stacking order, glycosyl torsion angles, loop type, and loop progression to allow for the creation of each unique quadruplex.

Introduction

In sequences of nucleic acid with particularly high proportions of guanine, four guanine bases can assemble themselves into a planar, four-stranded, Hoogsteen hydrogen-bonded structure. A single such structure is known as a G-tetrad. However, multiple G-tetrads can stack onto each other and adopt various loop configurations - producing a structure called a G-quadruplex. Though their full function is not completely understood, their high level of polymorphism and presence in critical sites of the human genome has piqued interest into their use as a possible target for small molecule anti-cancer drugs [1]. A set of accurate computational models for these structures then becomes a valuable tool for further research.

Any changes in one of the G-quadruplex properties - such as number of G-tetrads in the quadruplex, glycosyl torsion angles, position in the sequence, G-tetrad stacking order, DNA directionality, or loop progression - will result in a structurally unique quadruplex. Because of this possibility for variation, an enormous number of different quadruplexes can be created from a single sequence of DNA. The sheer number of permutations in this process makes an automated solution ideal. The goal of this project was to design a script that would take in a sequence of DNA and output every possible quadruplex that could be formed from that sequence.

To achieve this, two computer programs were developed: *Quadgen* and *Loopgen*, which would automate the processes of quadruplex formation and loop building respectively.

Methods

The flow of this project revolved around a two-step process of first manually effecting a change in a reference structure, then writing a computer script that would automate the process. The stepwise progression of this project was as follows:

1. Experimental coordinate values of a known quadruplex were taken and used to generate a starting model [2].
2. A survey of torsion angles and bond distances was taken from known quadruplexes 143D, 1KF1, 1XAV, 2GKU, 2HY9, 2JPZ, 2JSL, 2JSM, and 2KF8 using the AmberTools13 utility *cpptraj*. These torsions were used throughout the project to determine whether our artificially manipulated structures fell within acceptable ranges of known values.
3. The nucleic acid builder (nab) and Perl languages were used to write programs that could alter the various properties that differentiate between quadruplexes. (such as sugar torsion angle, stacking order, etc.)
4. The Perl script *Quadgen* was developed in order to choreograph these various nab programs and Perl subroutines. Its job is to take two reference tetrads and develop them into the full set of possible quadruplexes.
5. The structures produced by *Quadgen* were minimized in order to find their more low-energy forms.
6. Similar to step 2, a survey of torsion angles was taken from the loops of experimental quadruplexes.
7. Another Perl script, *Loopgen*, was written to take in one of the generated quadruplexes and use reference fragments to build the loops connecting each strand.

Quadgen Program Flow

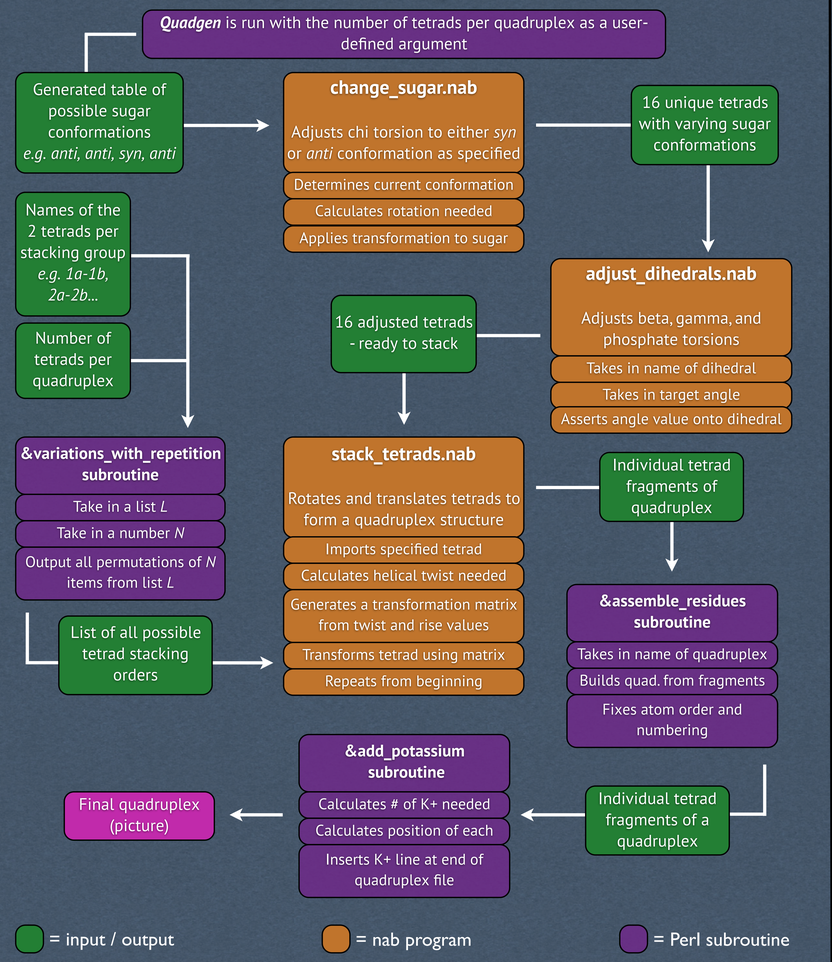

Loopgen Program Flow

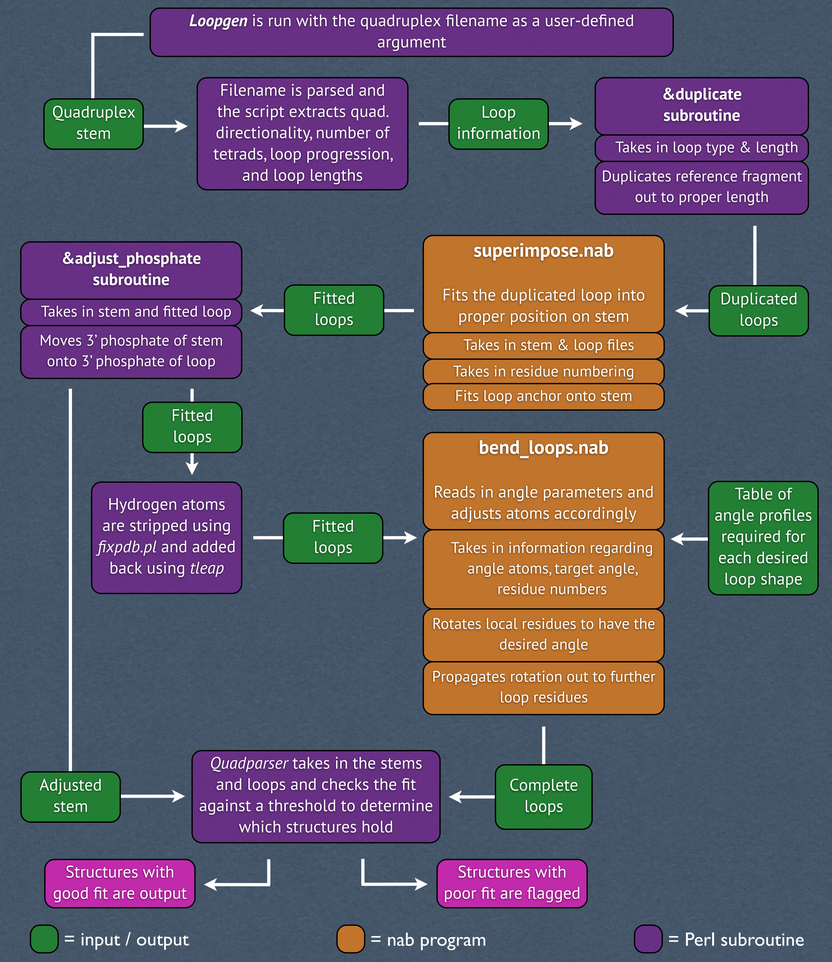

Sample Execution

Sequence

TGGGGAGGG
TGGGGAGGG
TGGGGAAGG

Possible quadruplexes (1D)
[415 possible structures]

....
TGGGGAGGGTGGGGAGGGTGGGGAAGG
TGGGGAGGGTGGGGAGGGTGGGGAAGG
TGGGGAGGGTGGGGAGGGTGGGGAAGG
TGGGGAGGGTGGGGAGGGTGGGGAAGG
TGGGGAGGGTGGGGAGGGTGGGGAAGG
TGGGGAGGGTGGGGAGGGTGGGGAAGG
TGGGGAGGGTGGGGAGGGTGGGGAAGG
TGGGGAGGGTGGGGAGGGTGGGGAAGG
TGGGGAGGGTGGGGAGGGTGGGGAAGG
TGGGGAGGGTGGGGAGGGTGGGGAAGG
TGGGGAGGGTGGGGAGGGTGGGGAAGG
TGGGGAGGGTGGGGAGGGTGGGGAAGG
...

Possible quadruplexes (3D)
[43935 possible structures]

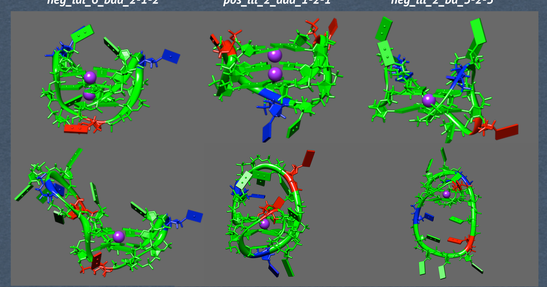

Conclusions

The programs were tested using the human *c-myc* nucleotide sequence. After a short round of minimization, the set of quadruplex models appeared to be structurally accurate and exhibit the full range of quadruplex polymorphism.

Despite structural accuracy, the relevancy of many of these quadruplexes is undetermined. The next step is to then examine the biophysical properties of these structures to determine if they exhibit those attributes that would make them valuable as possible molecular targets.

Acknowledgments

This project was funded by grant NIH/NCI R25-CA134283.

References

1. Le HT, Buscaglia R, Dean WL, Chaires JB, Trent JO, 2013, Calculation of Hydrodynamic Properties for G-Quadruplex Nucleic Acid Structures from *in silico* Bead Models, *Topics in Current Chemistry*, v. 330, pp. 179-210

2. Silva MW, 2007, Geometric Formalism for DNA Quadruplex Folding, *Chem. Eur. J*, v. 13, pp. 9738-9745

In vivo and *in vitro* determinates that regulate BCLxl's apoptotic potency

Amy Song and Levi J. Beverly

Department of Medicine, James Graham Brown Cancer Center
University of Louisville, Louisville, KY 40202, USA.

Abstract

BCLxl, a member of the B-cell lymphoma-2 (BCL-2) family, is a protein that plays a key role in cell survival by preventing mitochondrial outer membrane permeabilization (MOMP). The ability of BCLxl to block apoptotic signals in the cell has been positively linked to tumorigenesis. Previous *in vivo* experiments in the lab using mouse models showed the significance of individual domains within BCLxl's protein structure for dictating oncogenic potency. Specifically, the Bcl-2 homology (BH)-4 domain of BCLxl has been shown to be essential in the anti-apoptotic functionality of BCLxl. *In vitro* experiments were performed to analyze how altering the protein structure of BCLxl affected protein stability. Cells were transfected with chimeric BCLxl proteins and then treated with either a proteasome inhibitor (MG132) or a protein biosynthesis inhibitor (cycloheximide). Data showed that cells treated with cycloheximide significantly decreased the expression of BCLxl, whereas cells treated with MG 132 had no change or an increase in levels of protein expression. In contrast, treatment of chimeric BCLxl protein expression increased dramatically within 4 hours of MG132 treatment, but by 16 hours post-treatment, levels had decreased and returned to levels seen pre-treatment. Previous research has shown certain residues in the BH4 domain of Bcl-2 to be significant to the potency of the protein. Attempts were made to induce point mutations in the BH4 domain of BCLxl through site-directed mutagenesis. The data obtained from these analyses will be used to standardize results of future experiments.

Results

Intrinsic Apoptotic Pathway

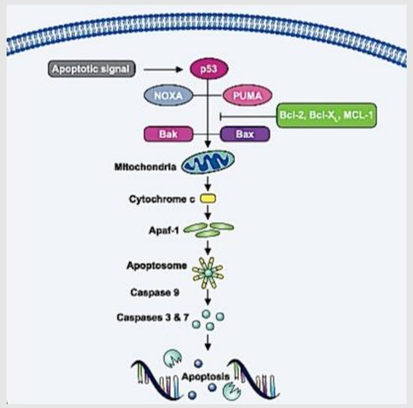

Figure 1. Intrinsic apoptotic pathway: directed by Bcl-2 protein mediation of mitochondrial outer membrane permeabilization.

BCLxl and BCLb Chimeric Constructs

Figure 2. Structures of BCLxl and BCLb and chimeric constructs. Construct 5 includes the BH4 and loop domains of BCLb; construct 7 only includes the loop domain of BCLb.

Survival Curves of *In vivo* BCLxl/BCLb Chimeric Constructs

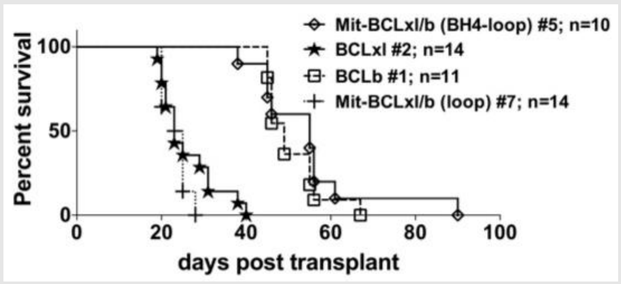

Figure 3. *in vivo* BCLxl/BCLb chimeric construct survival curves showing percent survival post transplant for mice infected with BCLb to be similar to those infected with construct #5, and separately, percent survival for those infected with BCLxl similar to those infected with construct #7.

Survival Curves of *In vivo* Transmembrane Domain Swap Constructs

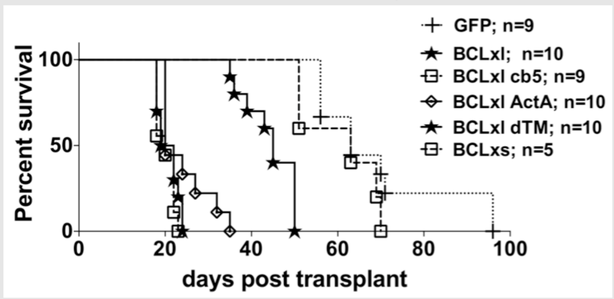

Figure 4. Percent survival post transplant of mice infected with BCLxl constructs with altered transmembrane domains. Percent survival of BCLxl and BCLxl cb5 are similar. BCLxl ActA shows a slight increase in survival.

In vivo expression of BCLxl constructs

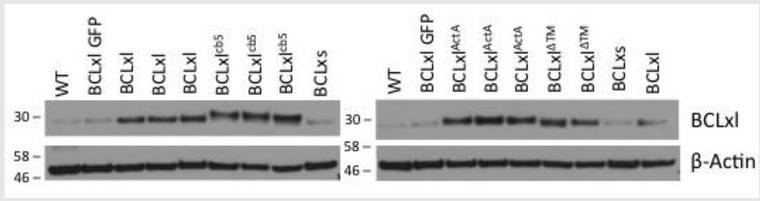

Figure 5. Western blot of *in vivo* BCLxl constructs. BCLxl, BCLxl cb5, and BCLxl ActA show a significant increase in levels of protein expression compared to wild type mice and those infected with BCLxl GFP or BCLxs.

Stability Test – MIT Constructs

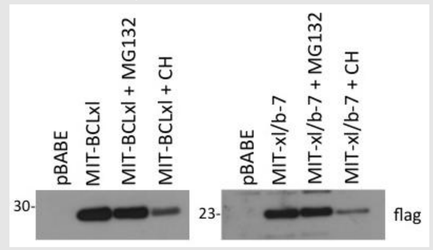

Figure 6. MIT constructs of BCLxl and construct 7 were treated for 16hrs with MG132 and cycloheximide. MG slightly decreased the levels of protein expression in BCLxl, with little change in construct 7, CH significantly decreased levels of protein expression.

Cycloheximide Time Course

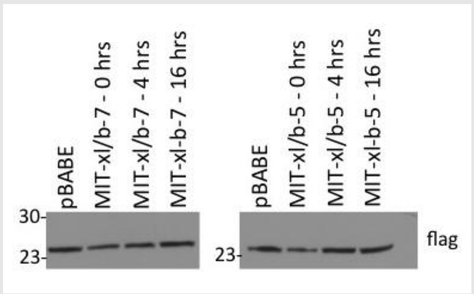

Figure 8. MIT constructs of constructs 5 and 7 were treated with cycloheximide for different periods of time. Levels of protein expression at time points 4 and 16hrs show a slight increase from initial protein levels.

Stability Test – CMV Constructs

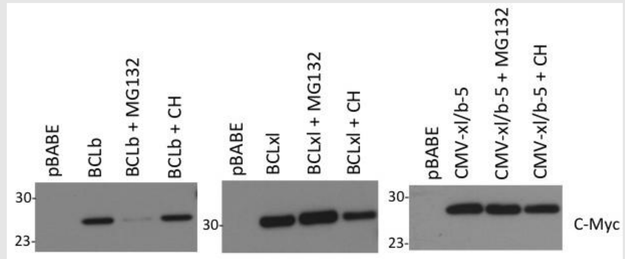

Figure 7. CMV constructs of BCLb, BCLxl, and construct 5 were treated with MG132 and cycloheximide for 16hrs. MG132 significantly decreases protein expression in cells transfected with BCLb and increasing expression in those with BCLxl. There's little change in levels of expression in construct 5.

MG132 Time Course

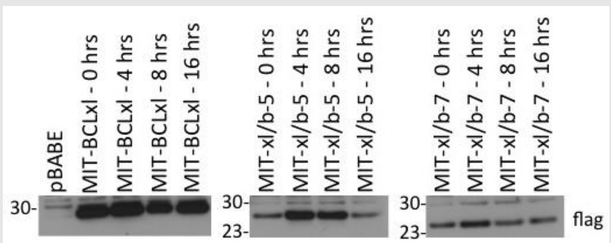

Figure 9. MIT constructs of BCLxl, construct 5 and 7 were treated with MG132 for different periods of time. The greatest increase in levels of protein expression is after 4hrs of treatment. After 8 to 16hrs, levels of protein expression return to initial levels.

Site Directed Mutagenesis

Figure 10. Point mutations of conserved residues in the BH4 domain of BCLxl are proposed to significantly impair the anti-apoptotic functionality of BCLxl. These mutations include replacements at the 6th, 9th, and 17th residues with glutamine, alanine, and tryptophan, respectively.

Conclusions

The various regulators of BCLxl's potency has been explored in both *in vivo* and *in vitro* environments. It can be seen that sequestering the protein to either the mitochondria or the endoplasmic reticulum through transmembrane domain swaps does not significantly affect the potency of BCLxl. Treatment with the protein biosynthesis inhibitor cycloheximide decreases protein expression in stability tests but this was not visible in the time course experiment. Treatment with the proteasome inhibitor MG132 results in a stabilization in protein levels for constructs 5 and 7 but the same result is not seen in BCLxl. Point mutations via site directed mutagenesis will be utilized in future experiments to further examine the potency of mutated BCLxl.

Acknowledgements

Research supported by grant R25-CA-134283 from the National Cancer Institute.
Many thanks to Dr. Levi Beverly and members of the Beverly lab, Lavona Casson, Parag Shah, Kumar Saurabh, Michael Scherzer, and Sean Shannon, for their mentorship and guidance.

Comparing target protein levels between non-neoplastic and sporadic CRC tissue based on dysregulated miRNAs

Vanessa States,[1] Steven Girdler,[1] Jonathan Rice, MD.,[1] Henry Roberts, BS.,[1] Maurice Eichenberger, MS.,[1]
Susan Galandiuk, MD.[1] Surgery.[1]

Introduction

- Colorectal cancer (CRC) is the third most common cancer worldwide. Early detection is key in successful CRC treatment.
- Dysregulated miRNA expression in known to play a role in carcinogenesis.
- Protein targets of miRNAs are potential therapeutic modalities.
  - PDCD4, PTEN, and TGF-β are protein targets of miRNA 21
  - RASA1 is a protein target of miRNA 31
- Previous results indicate miRNA expression in snap-frozen colon tissue significantly differs between non-neoplastic and cancerous samples.
- Formalin fixed paraffin embedded (FFPE) tissue is ideal for experimental use because it can be stored for an extended period of time
- Laser capture microdissection (LCM) is a technique that allows for the isolation of specific tissue sections and cell populations

Hypotheses

- Similar miRNAs will be significantly dysregulated in both fresh and FFPE (formalin fixed paraffin embedded) CRC tissue
- Proteins targets of dysregulated miRNAs will have different expression levels in CRC and normal tissue

Experimental Design

Cut serial sections of FFPE tissue

↓

Laser Capture Microdissection (LCM)

↓

miRNA Isolation

↓

qRT-PCR

↓

Protein Extraction

↓

Western Blot

Tissue from colon cancer patients was excised, fixed in formalin and embedded in paraffin. Serial sections (7 µm) were cut from FFPE tissue. Non-neoplastic and cancerous tissue was isolated from FFPE samples via LCM. miRNA was isolated from tissue. cDNA synthesis, pre-AMP and qRT-PCR were performed. Protein was extracted from remaining FFPE tissue for western blot analysis.

Results

qRT-PCR

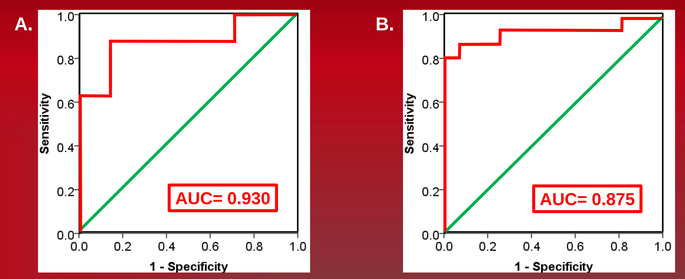

Figure 1. qRT-PCR analysis of coloncancer tissue. ROC curves for *miR-31, miR-135b, miR-1* and *miR-133a* combined for A.) snap frozen tissue and B.) FFPE tissue

microRNA	Fold Regulation Snap Frozen Tissue	Fold Regulation FFPE Tissue
miR-31	8.42	6.77
miR-135b	7.08	4.71
miR-21	3.42	2.13
miR-1	-4.35	1.51
miR-133a	-4.17	-1.00

Table 1. Fold regulation changes of snap frozen and FFPE tissue for *miR-31, miR-135b, miR-1* and *miR-133a.*

Western Blot

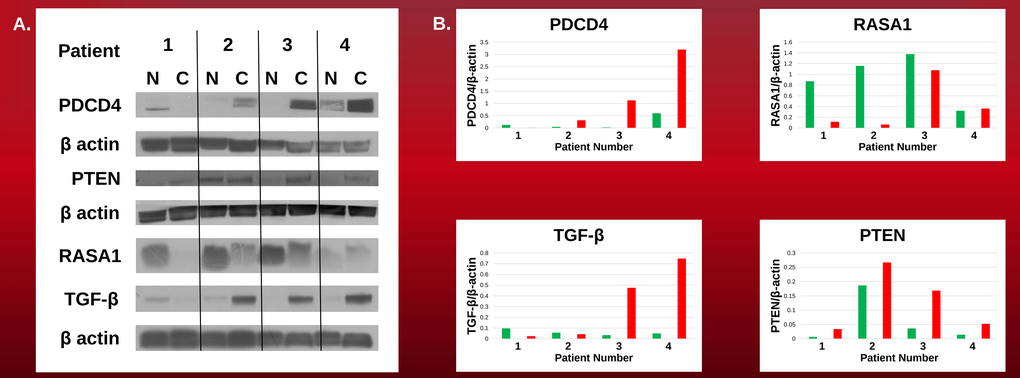

Figure 2.Western blot analysis of miRNA 21 and miRNA 31 protein targets. A. Representative western blot of PDCD4, PTEN, RASA1 and TGF-β in colon tumors and nonneoplastic tissue from four patients. B. Densitometry analysis of PDCD4, PTEN, RASA1 and TGF-β normalized to β-actin control. Protein extracts were prepared and 100 µg of tissue was loaded per lane on an SDS-PAGE.

N = non-neoplastic
C = cancerous

Key Findings

- Preliminary qRT-PCR data indicated that miR-31 and miR-21 were most dysregulated (upregulated) in cancer
- Protein extraction from FFPE tissue resulted in low yields
  - Probably due to molecular crosslinking from formalin fixation
- Western blot results inconclusive

Conclusions and Future Directions

- Slight differences in fold regulation between FFPE and snap frozen tissue may be due to miRNAs present in stroma
- Future protein analysis:
  - Optimize protein extraction from FFPE tissue
  - Use samples with same histological grade for western blot
  - Explore additional tumor suppressor pathways that may be affected by dysregulation of miRNAs

Supported by grant R25- CA-134283 from the National Cancer Institute.